Conduction and scattering mechanisms of the wurtzite In2Se3 crystals

Jazi Abdullah Mohammed Abdulwahed[1,*], S. A. Hussein[2], Khaled Ebnalwaled [3,4], A. Salem[2]

[1]Physics department, Umm Al-Qura University, College in Qunfudah – Female – KSA

[2] Solid State Lab., Physics Department, Faculty of Science, South Valley University, Qena 83523, Egypt

[3] Electronics & Nano Devices (END) lab, Physics Department, Faculty of Sciences, South Valley University, Qena 83523, Egypt

[4] Egypt Nanotechnology Center (EGNC), Cairo University Sheikh Zayed Campus, 12588 Giza, Egypt

* e-mail: jaabdulwahed@uqu.edu.sa

Abstract

In_2Se_3 crystals were prepared using modified Bridgman technique. The findings showed that the dominant conductive mechanisms are the thermionic emission and Mott variable range hopping. From the mobility measurements the scattering mechanisms are due to localized potentials and phonon scattering in the low and high temperature regions respectively. The findings of structural analysis at room temperature showed that the grown crystal match α-phase structure. The dependence of Hall effect, electrical conductivity, Hall mobility and charge carriers concentration on temperatures revealed the presence of α - to β - phase transition at about 467 K. Structural, localized states and transport parameters were calculated for the prepared crystals. The crystals obtained have greater mobility of the charge carrier, thermoelectric power, and power factor than other reported results.

Keywords: Phase transition, transport properties, conduction mechanism, scattering mechanism, power factor.

1- Introduction

In_2Se_3 is a $A_2^{III}B_3^{IV}$ has favorable optical and electrical properties [1, 2]. In_2Se_3 is an attractive semiconductor for its potential applications: batteries [3-6], photovoltaic cells [7-11], PRAM [12, 13] and electrothermal devices [14].

Many papers have dealt with the ordering of In_2Se_3 [14- 16] and it was found that it can have five different phases including *α, β, γ, k* and *δ* phases.

The layered structure (*α*-phase) constructs from wide stacks of covalently bonded layers, including five atomic layers of Se-In-Se-In-Se, by van der Waals force. The layered In_2Se_3 is a structure ordered by vacancies; its basic structure is the structure of Wurtzite or zincblende. *β*- In_2Se_3 is a metastable structure obtained from *α*- In_2Se_3 by heating and will be transformed back to *α*- In_2Se_3 at room temperature unless doped with Sb, which makes it stable even though the heating is terminated [17]. Meanwhile, the defect wurtzite structure (*γ* – phase) is a wurtzite structure, but ½ of the cation sites are vacant like the defect zincblende structure [18, 19]. After annealing, the metastable anisotropic structure of k- In_2Se_3 was obtained on the surface of *λ*- In_2Se_3. This structure is distinct but similar to *α*- In_2Se_3 [20]. To stabilize k- In_2Se_3 [21] some group doped Zn. Eventually, it is possible to obtain ÿ- In_2Se_3 at high temperature and shows hexagonal structure [22]. Understanding the conduction and scattering mechanisms are crucial to the successful applications of the materials. So the aim of this research is to investigate the conduction and scattering mechanisms. Different structural and transport parameters were extracted which may be opened up the possibilities of new practical applications for In_2Se_3 crystals.

2- Experimental arrangement

a. Sample preparation

In_2Se_3 crystals were grown by a modified Bridgman technique. Stoichiometric amount from high purity (6N) indium and selenium were sealed in a quartz ampoule under a vacuum of 10^{-6} Torr. The sealed ampoule was placed into a furnace. At the beginning of the growth run, the furnace temperature was raised to 1150 K and let there for 36 h. The ampoule was then moved into the crystallization zone, which its temperature was adjusted according to the phase diagram [23]. The ampoule was kept there for 24 h. In the solidification zone, the ampoule was cooled slowly by a rate of 2 mm/h till it reached the room temperature. The obtained crystals have black shiny color, which is the distinguish color for α – In_2Se_3 crystals [24].

b. Sample characterization

D 5000 Siemens diffractometer (Germany) was used to investigate the crystal structure of the prepared crystals by analyzing X-ray diffraction (XRD) patterns measured Progress by 0.02°, at room temperature.

To research the chemical composition of the grown crystals, Elemental Analyzer EDXRF, JSX3222, JEOL, (Japan) was used. The Hall effect and dc electrical conductivity measurements were measured in an evacuated cryostat; the sample dimension was adjusted to be 9 x 3 x 2.7 mm^3.

Samples have 5 mm length and 8 mm diameter were used to investigate the thermoelectric coefficient in an evacuated calorimeter.

To assess the conductivity, an interfaced Hioki 3532-50 LCR Hi-tester with a frequency range of 42 Hz to 5MHz was used in a device. The measurements were performed by keeping the sample (5mm thickness, and 8 mm diameter) between two stainless steel electrodes in an evacuated and temperature-controlled chamber. The input parameters were varied by means of completely computer-controlled software appended to the LCR meter.

The silver conducting paste was used as a contact material to measure the dc electrical conductivity, Hall effect, thermoelectric power and ac electrical conductivity. The measurements of I – V curves in forward and reverse directions confirm the ohmic nature of the used contacts.

3- Results and discussion

3.1 Structural characterization

The EDX analysis was made at different areas of the sample and it was found that the samples are composed of In and Se only, no other impurities were detected. This assured that the composition was uniform throughout the sample. The variations in composition from one area to another never exceed 0.2 % of the measured values.

The XRD pattern for the sample being grown is shown in Fig. 1. Indexing and refinement of XRD pattern confirm that the grown sample crystallized to wurtizite structure (α – In_2Se_3) with the reflection arising from 004, 006, 110, 0010, 0014 and 1114 planes. XRD measurements showed agreement with Cross-Ref PDF No. 34 – 1279 (Fig. 1 inset).

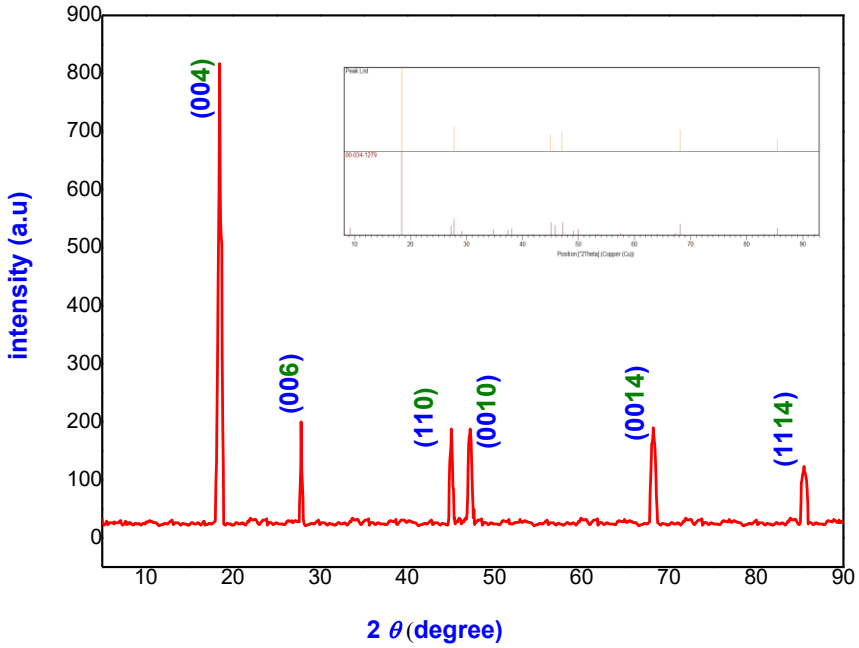

Fig. 1: XRD spectra of In_2Se_3 crystals

Table 1 gives a comparison between interplanar spacing (d_{hkl}) for the obtained In_2Se_3 crystals and d_{hkl} for the standard hexagonal α - In_2Se_3 crystals [25]. The standard and calculated d_{hkl} of the diffraction lines are found to be consistent.

d_{hkl} for the obtained crystal	d_{hkl} for the hexagonal α-In_2Se_3 crystals [25]
4.82	4.81
3.206	3.205
2.016	2.011
1.931	1.923
1.375	1.374
1.135	1.135

Table 1: A comparison between d_{hkl} for the obtained In_2Se_3 crystals and d_{hkl} for the standard hexagonal α - In_2Se_3 crystals

The parameters a and c of the lattice are calculable from:

$$\frac{1}{d_{hkl}^2} = \frac{4}{3}\left[\frac{(h^2 + hk + k^2)}{a^2}\right] + \frac{l^2}{c^2} \qquad 1$$

where *h*, *k*, *l* are the lattice planes. The values of *a* and *c* calculated from each diffraction line are treated by an angular function of $\cos^2\theta$-type **[26]** to obtain the accurate lattice parameters. From Fig. 2, the lattice parameters for the obtained In_2Se_3 crystals are a = 4.031 ± 0.004 Å and c = 19.267 ± 0.002 Å. These values are close to the corresponding values reported for α - In_2Se_3 hexagonal (a = 4.025 Å and c = 19.23 Å) **[25]**, That confirms the identification between regular and prepared crystals.

Crystallite size (D) of the obtained In_2Se_3 crystals was calculated to be 29 nm from the Debye Scherrer's formula from the full width at half-maximum (FWHM) β of the peaks expressed in radians **[27]**:

$$D = \frac{0.94\lambda}{\beta\cos\theta} \qquad 2$$

where λ is 1.54056 Å for Cu Ka and θ is the Bragg angle.

In spite of the accuracy of Scherrer equation, it neglects the importance of the microstrain, ε, and its effects in the diffraction pattern [28]. Williamson–Hall (WH) plot was used to separate the broadening of the XRD peaks according to crystallite size and microstrain [29]:

$$\frac{\beta}{\lambda}\cos\theta = \frac{k}{D} + \frac{4\varepsilon}{\lambda}\sin\theta \qquad 3$$

Figure 3 shows the WH plotting for In_2Se_3 crystals. From the figure, the average crystallite size D = 28.66 ± 0.03 nm and the microstrain is about 0.0031 ± 0.0001. The positive signal of the microstrain confirms the obtained results from Fig. 2, that there is a lattice expansion.

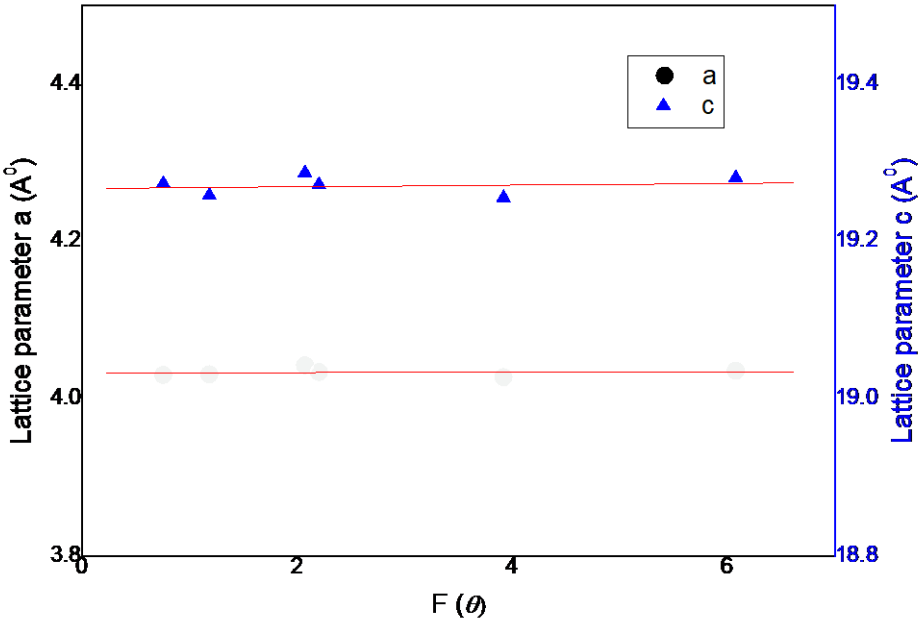

Fig. 2 The relation between the lattice parameters and *F(θ)*

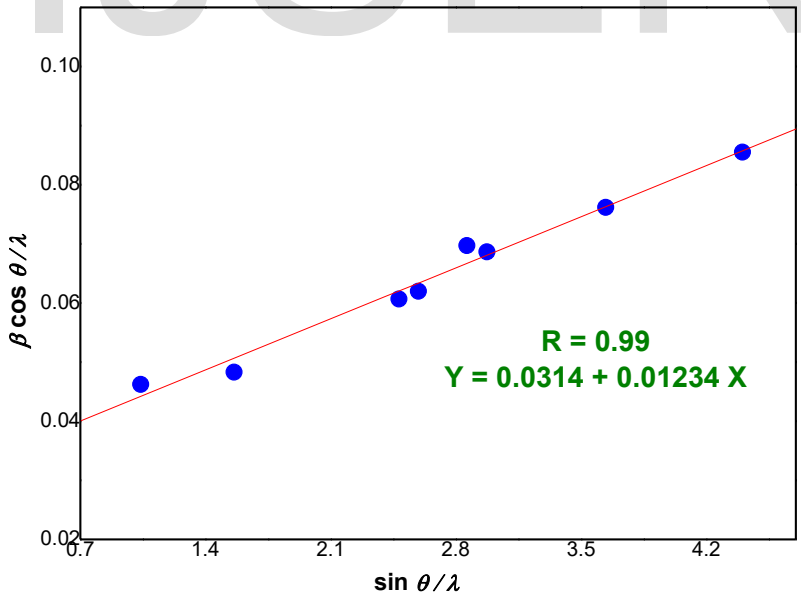

Fig.3: WH plot for In_2Se_3 crystals

3.2 dc conductivity studies

The variations of dc conductivity as a function of $10^3/T$ in the temperature range 250 - 560 K are illustrated in Fig.4. The electrical conductivity was found to be 6.35 Ω^{-1} cm^{-1} at room temperature. This value is greater than other published data [30 - 35].

In general the conductivity is raised with increasing the temperature in the extrinisic conduction region 255 K ≤ T < 300 K. In the transition region 300 K ≤ T < 414 K, the conductivity is grown slowly with temperature. In the intrinsic region 414 K ≤ T < 467 K, the conductivity is increased rapidly with temperature, while as the temperature reach 467 K the conductivity is decreased with increasing the temperature. This is may be due to the phase transition from α – In_2Se_3 to β – In_2Se_3 which happen near 473 K [36]. It's known that α – In_2Se_3 more conductive than β – In_2Se_3 [37].

As it has been found that In_2Se_3 crystals are N-type semiconductor, this finding is in good agreement with published data [29 - 38]. As known $A_2^{III}B_3^{IV}$ crystals have excess of cations which act as donor centers [39]. The following Arrhenius relations were used to examine the behavior of dc conductivity for the prepared crystals **[**40**]**:

$$\sigma = \sigma_0 \exp(-\Delta E_d / 2K_B T) \quad \text{(Extrinsic conduction)} \quad 4$$

$$\sigma = \sigma_0 \exp(-\Delta E_g / 2K_B T) \quad \text{(Intrinsic conduction)} \quad 5$$

where σ is the conductivity, σ_0 is a pre – exponential factor, K_B is the Boltzmann constant, ΔE_d is the activation energy, ΔE_g is the energy gap width and T is the absolute temperature. From the above relationships ΔE_d is calculated to be 0.49 ± 0.02 eV and ΔE_g is 1.14 ± 0.01 eV. These values are in good agreement with reported values by other authors **[**1, 30 and 35**]**.

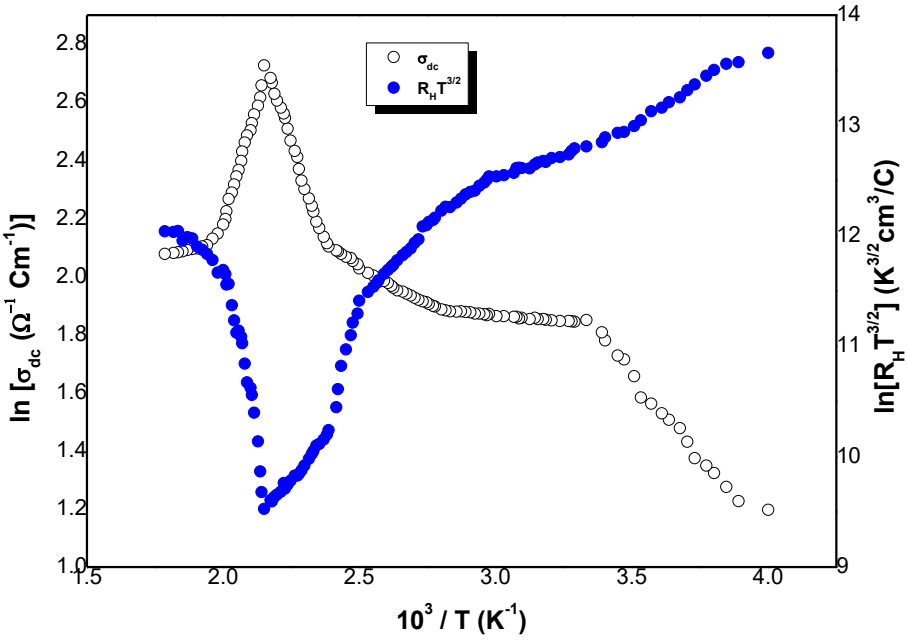

Fig.4: The variations of the dc electrical conductivity and ln$R_H T^{3/2}$ as a function of inverse temperature for In_2Se_3 crystals.

3.3 Scattering mechanism

The Hall effect was investigated in the same temperature range of dc electrical conductivity. The conduction type of In_2Se_3 was determined from the Hall effect measurements and was found to be a N – type semiconductor. The relationship between ln (R_H. $T^{3/2}$) and $10^3/T$ was plotted in Fig. 4. By analyzing the R_H data, the depth of the donor level was found to be 0.58 ± 0.02 eV while the energy gap width was 1.3 ± 0.02 eV.

From the figure, at low temperatures the Hall coefficient shows less rapid dependence on the temperature, by increasing the temperature, the sample shows a considerable fall of the Hall coefficient. The Hall dip at 467 K and the increase of the Hall coefficient after this temperature is due to the phase transition from α to β In_2Se_3 [37].

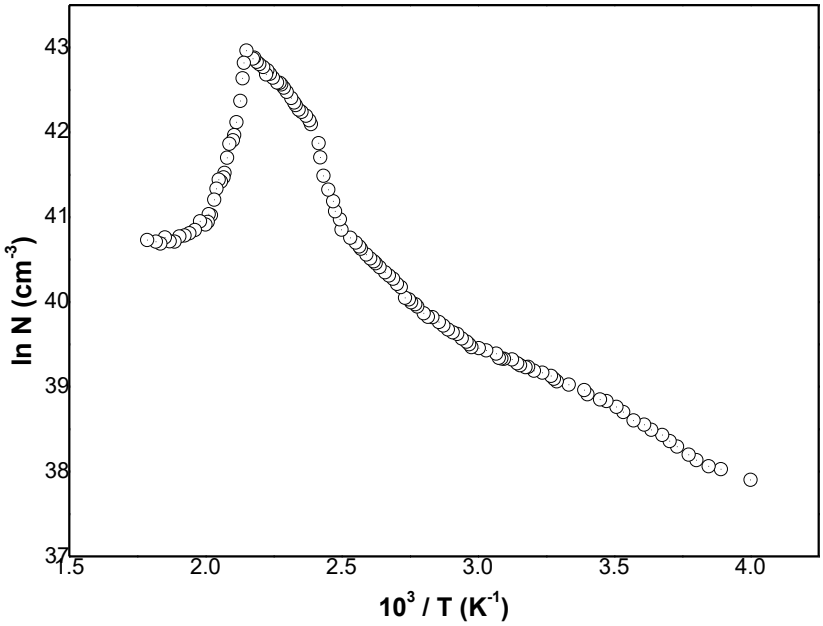

Fig.5: Density of charge carrier vs. 10^3/T for In_2Se_3 crystals

The variation of charge carriers density verse reciprocal temperature is illustrated in Fig. 5. As the temperature is increased the charge carrier density is increased, till 467 K, after this temperature the charge carrier density is decreased with increasing the temperature. This another evident that at 467 K, there is a phase transition from α- to β – In_2Se_3. The charge carrier concentration at room temperature is 8.872 x 10^{16} cm^3, which is higher than published results [34, 36]; this may be attributed to the disorder nature of our sample [34].

Based on the obtained results of the electrical conductivity and Hall effect, we investigate the influence of temperature on Hall mobility for the grown In_2Se_3 crystals. This is presented in Fig. 6. As shown from the figure, the mobility is decreased with the temperature in the extrinsic and transition regions, and slightly increased with temperature in the intrinsic region.

While after the phase transition temperature, 467 K, the mobility is sharply increased with temperature. The room temperature Hall mobility is 447 cm^2 / V. s, which is greater than other published data [29 - 38].

The dependence of μ and T justifies the following relationship $\mu \alpha T^{-1.4}$ in the extrinsic region. Such dependence leads to the assumption that the scattering mechanism is due to the localized potentials in this range. At high temperature (intrinsic region) μ and T follow the relation $\mu \alpha T^{1.5}$ this relation leads to that the scattering mechanism is due to the phonon scattering in this range [34].

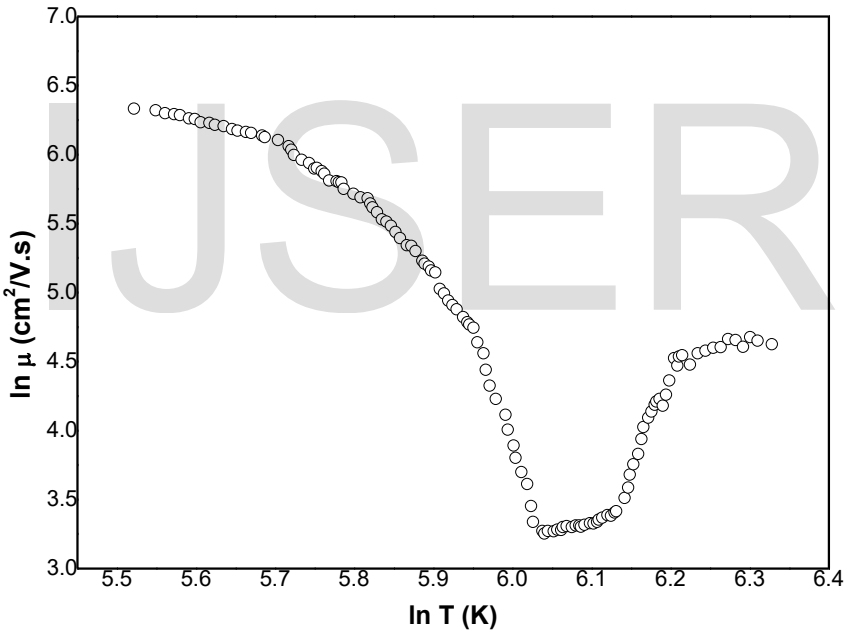

Fig. 6: Hall mobility as a function of temperature for In_2Se_3 crystals

3.4 Conduction mechanism

To reveal the dominant conduction mechanism in the grown In_2Se_3 crystal, the conductivity – temperature dependence was analyzed. Fig. 7 shows the electrical conductivity in the low temperature region as a function of $T^{-1/4}$. A

linear dependence between the conductivity and $T^{-1/4}$ establishes that the conduction mechanism may follow the Mott's variable range hopping (MVRH) model **[**41, 42**]**. According to MVRH model, the dc conductivity is proportional to exp $(-T_0 / T)^{1/4}$, T_0 being the characteristic temperature.

The Mott temperature T_0, the density of states at Fermi level $N(E_f)$, the average hopping distance R_{hop} and the average hopping energy *W* can be calculated according to the following equations:

$$\sigma\sqrt{T} = \sigma_1 \exp(\frac{-T_0}{T})^{1/4} \quad (6)$$

$$\sigma_1 = \frac{e^2 \gamma_{ph} N(E_f)}{\gamma} \quad (7)$$

$$T_0 = \frac{\beta}{K_B N(E_F) R_{hop}^3} \quad (8)$$

$$R_{hop} = \left(\frac{9}{8\pi\gamma K_B T N(E_F)}\right)^{1/4} \quad (9)$$

$$W = \frac{3}{4\pi R_{hop}^3 N(E_F)} \quad (10)$$

where γ is the decay constant, $\gamma_{ph} \sim 10^{13}$ s^{-1} is the phonon frequency, β is dimensionless constant. The calculated parameters (table 2) were found to achieve Mott's requirements ($T_0 > 10^3$K, $\gamma R_{hop} > 1$, $W > K_B T$) for variable hopping to dominate.

From Fig. 7 the variation of Hall mobility follows a $T^{-1/4}$ dependence in the low temperature region. This indicates that Hall mobility is based on an averaging procedure of spatial and energetically disordered hopping system [43].

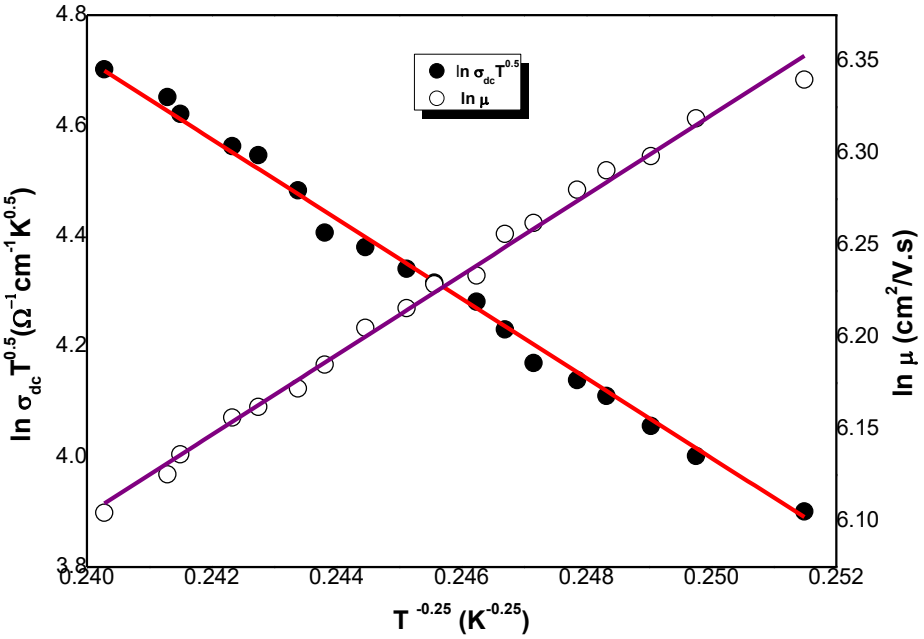

Fig. 7: ln σ_{dc} and ln μ vs. $T^{-1/4}$ for In_2Se_3 crystals.

By utilization from the obtained results, the scattering energy of trap states near Fermi level and the concentration of trapping states have been calculated according to [42] and were found to be 0.251 eV and 9.86 x 10^{18} cm^{-3} respectively.

The atomic disorder degree (T_0 / T) is calculated to be 1.43 x 10^{5} at room temperature. The high value of the atomic disorder degree is attributed to that the alternating Se and In layers along the *c* axis have a repeat of the form Se – In – Se – In – Se and two such units form the unit cell with a hexagonal packing SeInSeInSe InSeInSe such type of structure increases the density of localized states near the Fermi level [31, 32].

From the above results, it is obvious that the conduction mechanism in the low temperature region is due to Mott variable range hopping. The other hopping mechanism which considers coulomb interactions does not fit the

experimental results, since coulomb interactions is observed in heavily doped semiconductors.

The conduction mechanism is due to thermionic emission of charge carrier at high temperature [44]. The change of conduction mechanism from thermionic emission to Mott variable range hopping may be due to that the bonding inside the layers is strongly covalent, while the interlayer interaction (Se – Se) is of the van der waals type, which lead to presence of Se vacancies due to faulting of the neighboring Se – Se layers.

3.5 ac conductivity studies

Using the values of the conductance, G, measured by the LCR meter over a frequency range of 42 to 5 MHz and a temperature range 298 K to 493 K, the ac conductivity (σ_{ac}) has been calculated:

$$\sigma_{ac} = \frac{Gd}{A} \qquad 11$$

where d is the sample thickness and A is the cross sectional area.

Fig. 8 shows the typical ac conductivity behavior of In_2Se_3 crystals at different temperatures. At low frequencies, the sample conductivity is frequency independent. This is due to the random diffusion of charge carriers via hopping [45]. At high frequencies the sample conductivity is increased with increasing the frequency. As the temperature increased the ac conductivity is increased till reaching the phase transition temperature 467 K the conductivity is decreased with temperature. This result is in good agreement with dc conductivity results.

The transfer from the frequency – independent to frequency – dependent region is an indication of onset of conductivity relaxation **[**46**]**.

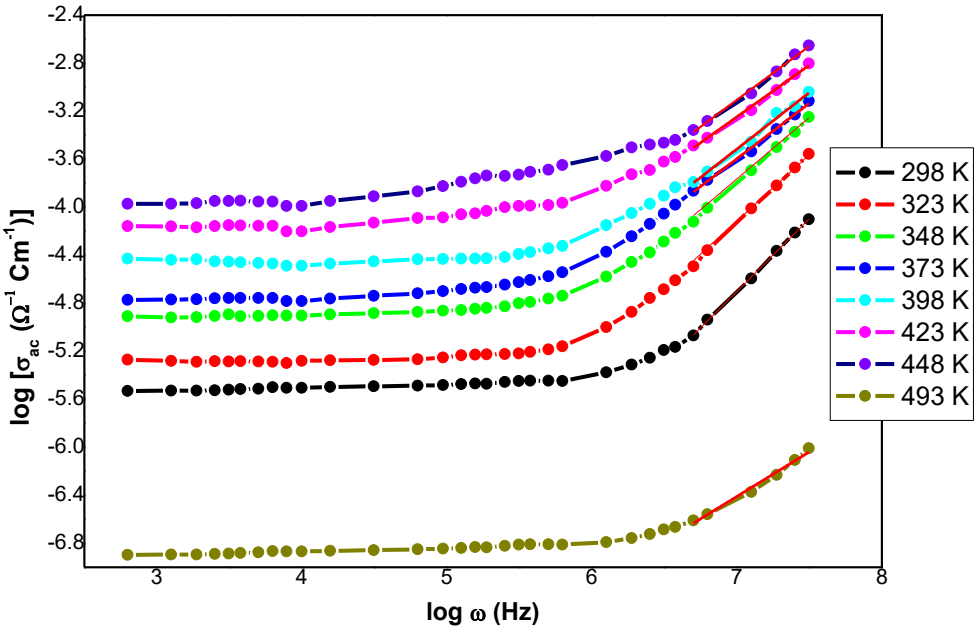

Fig. 8: The plot of log σ_{ac} vs. log ω.

For semiconductors the ac conductivity follows the power law behavior **[**47**]**:

$$\sigma_{ac}(\omega) = A\omega^{s} \qquad 12$$

where A is temperature dependent constant and *s* is the frequency exponent and ω is angular frequency. As indicated from Fig. 9 (a) the value of *s* is < 1 and decreases with temperature, which revales that the conduction is due to correlated barrier hopping (CBH) **[**48 – 51**]**.

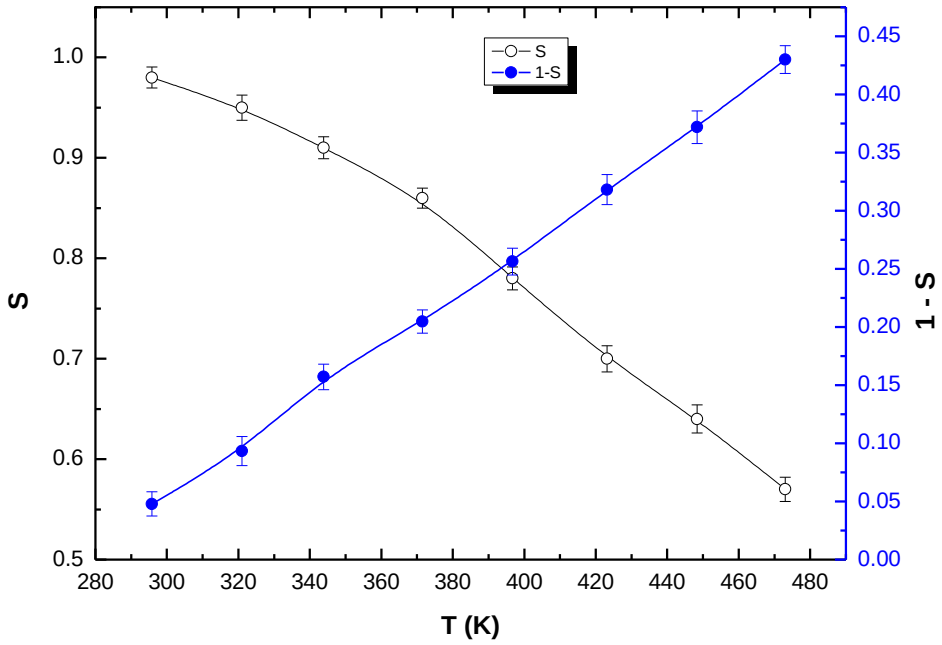

Fig. 9 Temperature dependence of the frequency exponent s and 1-s

CBH model suggests hopping of electron pairs from a doubly occupied D^+ state to a D^- state over a barrier separating the two different states. So according to the CBH model the exponent *s* can be directly correlated to the barrier height (W_m) by the following relation

$$1 - s = \frac{6K_B}{W_m} T \qquad 13$$

The obtained value of W_m (table 2) is agreed with the calculated value from Mott's theory.

Fig. 10 shows the relation between ac conductivity and the reciprocal temperature at different frequencies for In_2Se_3 crystals. It is clear from the figure that σ_{ac} increases with increasing the temperature; this indicate that the ac conductivity is a thermally activated process from different localized states in the gap or its tails **[**52**]**. At T > 464 K the σ_{ac} decreased. This is

corresponds to the same behavior of σ_{dc} and confirm the phase transition from α – to β – In_2Se_3 phase.

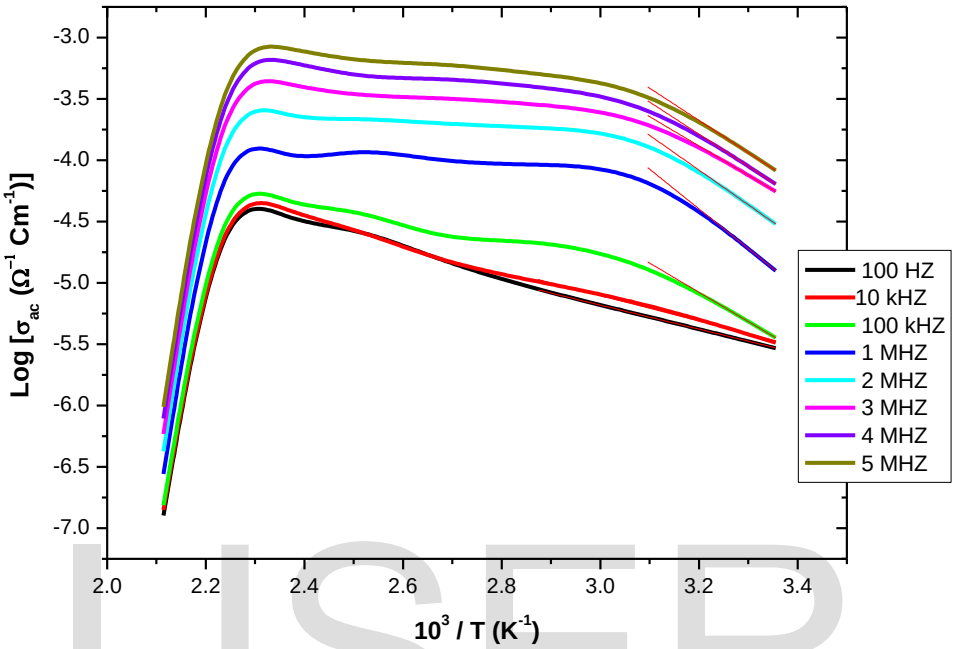

Fig. 10: Temperature dependence of σ_{ac} (ω) for In_2Se_3 crystals.

The activation energy ΔE (ω) is obtained at different frequencies using the well – known equation:

$$\sigma_{ac} = \sigma_0 \exp(\Delta E(\omega)/K_B T) \qquad 14$$

Fig. 11 illustrates the frequency dependence of ac activation energy for In_2Se_3 crystals. It is clear that ΔE (ω) decreases with increasing frequency. Such a decrease can be attributed to the jump of charge carriers between the localized states by the increase of the applied field, which lead to the activation energy ΔE (ω) decreases with increasing the frequency **[**53**]**.

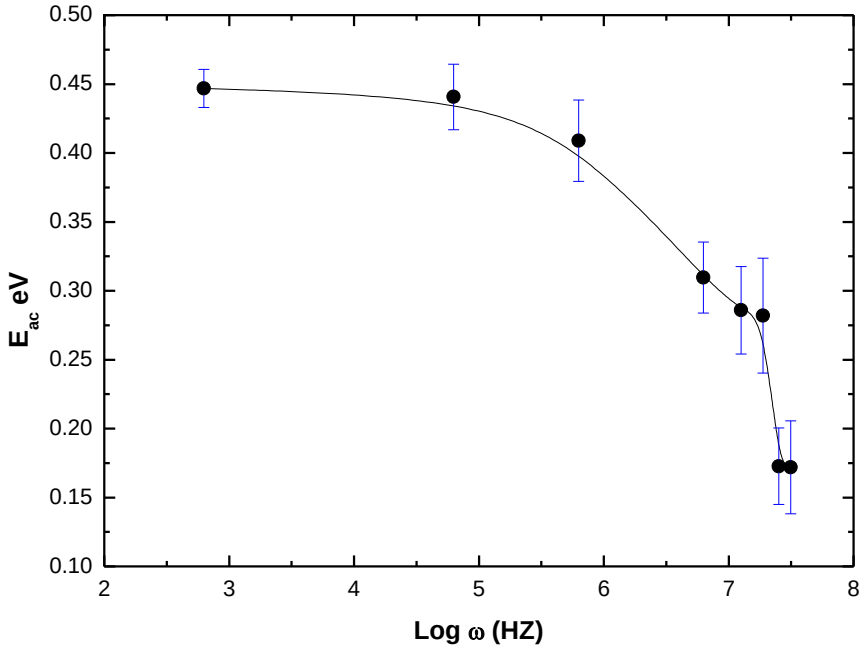

Fig. 11: Frequency dependence of the ac activation energy for In_2Se_3 crystals.

The smaller values of the ac activation energy and the decrease of ΔE (ω) with frequency indicate that the hopping conduction is predominant conduction mechanism **[**49 – 51, 54**]**.

3.6 Seebeck coefficient measurements

The behavior of Seebeck coefficient for the obtained In_2Se_3 crystals against temperature has been investigated and shown in Fig. 12. Generally the Seebeck coefficient α increases with temperature till it reaches its maximum value 0.38 mV/K at 467 K, after that α is decreased rabidly with temperature. This is due to the phase transition from α – to β - In_2Se_3.

The Seebeck coefficient measurements confirm that the grown In_2Se_3 crystals is N – type, since the sign of α is negative. The value of α at room

temperature is 0.261 mV/K, which is higher than other published data [56, 57].

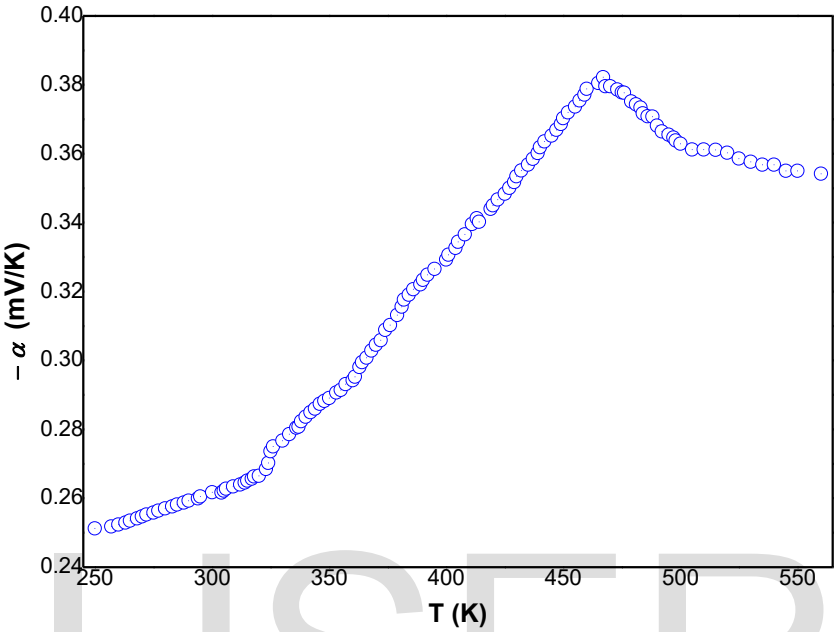

Fig. 12: Variation of Seebeck coefficient as a function of temperature for In_2Se_3 crystals

According to the following equation [58]:

$$\alpha = \frac{3}{2}\frac{K_B}{e}\ln T + const. \qquad 15$$

The straight-line slope of a plot of α against ln T, for a given sample was found to be higher than the theoretical prediction (129 μVK^{-1}), which indicates that the effective masses of the charge carriers are temperature dependent for In_2Se_3 crystals [59].

As known the dimensionless thermoelectric figure of merit Z is equal to $\alpha^2\sigma$ /k, where k is the thermal conductivity; so large power factor $\alpha^2\sigma$ and low thermal conductivity is required for high figure of merit materials for thermoelectricity applications. By combining α and σ results the power

factor, $\alpha^2\sigma$, for thermoelectric conversion was obtained as a function of T for In_2Se_3 crystals, Fig. 13. The power factor reaches the maximum value at 467 K, about 2.21 mW/cm.K^2. The obtained value is better than the published data for In_2Se_3 [56, 57] and is appropriate compared with published results for other thermoelectricity materials [60].

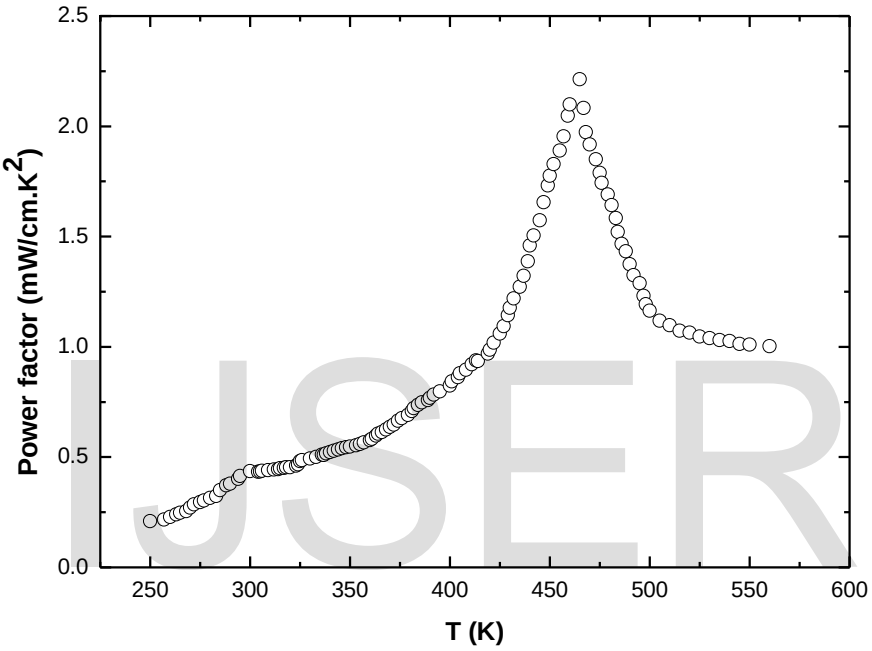

Fig. 13: The variation of the power factor with temperature for In_2Se_3 crystals.

Parameter	Value
σ_{dc} (Ω^{-1} cm^{-1})	6.35
T_o (K)	4.3 x 10^7
$N(E_f)$ (cm^{-3} eV^{-1})	3.92 x 10^{19}
R_{hop} (cm)	3.65 x 10^{-7}
γ (cm)	2 x 10^7
γR_{hop}	7.29
W (eV)	0.126
W_m (eV)	0.14
m_n (Kg)	1.9 x 10^{-34}
m_p (Kg)	2.2 x 10^{-34}

t_n (s)	1.06×10^{-12}
t_p (s)	1.11×10^{-12}
D_n (cm^2/s)	11.6
D_p (cm^2/s)	10.5
L_n (cm)	3.5×10^{-6}
L_p (cm)	3.3×10^{-6}
μ_n (cm^2 / V. s)	447
μ_p (cm^2 / V. s)	407
N (cm^3)	8.87×10^{16}
α (mV/K)	0.261
$\alpha^2\sigma$ ($mW/cm.K^2$)	0.44

Table 2: Localized states and transport parameters for the grown α - In_2Se_3 crystals at room temperature

4. Conclusion

α - In_2Se_3 crystals have been grown by modified vertical Bridgman technique from stoichiometric melts. The prepared crystals exhibit α – to β-phase transition at 467 K. Mott variable range hopping and thermionic emission are the conduction mechanisms at the low and high temperature respectively for dc electrical conductivity. Correlated barrier hopping is the dominate conduction mechanism for ac electrical conductivity. The scattering mechanism at low temperatures is due to localized potentials, while at high temperatures is due to phonons. The grown crystals have charge carrier mobility, thermoelectric power and power factor higher than other published data.

References

[1] Julien C., Chevy A., Siapkas D., *Phys Stat Sol (a)*, 118 (1990), 553.

[2] Yudasaka M., Matasuoka T., Nakanishi K., *Thin Solid Films*, 146 (1987), 65.

[3] Julien C., Samaras I., Tsakari M., Dzwonkowski P., Balkanski M., *Mater. Sci. Eng. B*, 3 (1989), 25.

[4] Samaras I., Saikh S. I., Julien C., Balkanski M., *Mater. Sci. Eng. B*, 3 (1989), 209.

[5] Balkanski M., Julien C., Emery, *J. Power Sources*, 26 (1989) 615.

[6] Julien C., Massot M., Dzwonkowski P., Emery J. Y., Balkanski M., *Infrared Phys.*, 29 (1989), 169.

[7] Kenawy M. A., Zayed H. A., El-Soud A. M. A., *J. Mater. Sci.: Mater. Electron.*, 1 (1990), 115.

[8] Segura A., *II Nuovo Cimento B*, 38 (1977), 345.

[9] Julien C., Lithium insertion in chalcogenides: electrochemical properties and electrodes applications, in Microionics Solid State Integrable Batteries (EUR 1267 EN), Balkanski, Paris, 1991, p 309.

[10] Lakshmikumar S. T., Rastogi A. C., *Solar Energy Mater. Solar Cells*, 32 (1994), 7.

[11] Segura A., Chevy A., Guesdon J. P., Besson J.M., *Sol. Eng. Mater.*, 2 (1980), 159.

[12] Lee H., Kang D.-H., Tran L., *Mater. Sci. Eng. B*, 119 (2005), 196.

[13] Baek C. K., Kang D., Kim J. S., Jin B., Rim T., Park S., Meyyappan M., Jeong Y. H., Lee J. S., *Solid-State Electronics*, 80 (2013), 10.

[14] Julien C., Eddrief M., Kambas K., Balkanski M., *Thin Solid Films*, 137 (1986), 27.

[15] Kim H. G., Min I. S., Kim W. T., *Solid State Comm*., 46 (1987), 819.

[16] Pfitzner A., Lutz H. D., *J Solid State Chem*, 124 (1996), 305.

[17] Emziane M., Marsillac S., Bernede J.C., *Mater. Chem. Phys.*, 62 (2000), 84.

[18] Jiping Y. E., Soeda S., Nakamura Y., Nittono O., *Jpn. J. Appl. Phys.*, 37 (1998), 4264.

[19] Eddike D., Ramdani A., Brun G., Tedenac J.C., Liautard B., *Mater. Res. Bull.*, 33 (1998), 519.

[20] Swider J. J. W., Washburn J., Liliental-Weber Z., Chaiken A., Nauka K., Gibson G. A., Yang C. C., *Appl. Phys. Lett*, 81 (2002), 23.

[21] Chaiken A., Nauka K., Gibson G. A., Lee H., Yang C. C., Wu J., Ager J. W., Yu K. M., Walukiewicz W., *J. Appl. Phys.*, 94 (2003), 4.

[22] Huang Y. C., Li Z.Y., Uen W.Y., Lan S. M., K. J. Chang, Xie Z.J., Chang J.Y., Wang S. C., Shen J. L., *J. Cryst. Growth*, 310 (2008), 1679.

[23] Immi K., Suzuki K., Haga T., Hasegawa Y., Abe Y., *J. Cryst. Growth*, 54 (1981), 501.

[24] Ho C.-H., Lin M.-H., Pan C.-C., *Sensors and Actuators B*, 209 (2015), 811.

[25] Popovic S., Tonejc A., Plenkovic B. G., Celustka B., Trojko R., *J. Appl. Crtst*. 12 (1979), 416.

[26] Varin R. A., Bystrzycki J., Calka A., *Intermetallics*, **7** (1999), 917.

[27] Scherrer P., Gottingen N.G.W., *Math-Pys. Kl.*, 2 (1918), 96.

[28] Markmann J., Yamakov V., Weissemüller J. , *Scr Mater*, 59 (2008) 15.

[29] Williamson G. K., Hall W. H., *Acta Metall*, 1 (1958).

[30] Julien C., Eddrief M., Balkanski M., Hatzikraniotis E., *Phys. Stat. Sol. (a)*, 88 (1985), 687.

[31] Julien C., Hatzikraniotis E., Kambas K., *Phys. Stat. Sol. (a)*, 97 (1986), 579.

[32] Julien C., Balkanski M., *Mater. Sci. Eng. B*, 38 (1996) 1.

[33] Fotsing J., Julien C., Balkanski M., Kambas K., *Mater. Sci. Eng. B*, 1 (1988), 139.

[34] Boledzyuk V. B., Zaslonkin A. V., Kovalyuk Z. D., Pyrlya M. M., Ukr. *J. Phys.*, 56 (4) (2011), 376.

[35] Kaminskii V. M., Kovalyuk Z. D., Zaslonkin A. V., Ivanov V. I., Semiconductor Physics, Quantum Electronics & Optoelectronics, 12 (3) (2009), 290.

[36] Blasi C. D., Drigo A. V., Micocci G., Tepore A., Mancini A. M., *J. Cryst. Growth*, 94 (1989), 455.

[37] Kim H. – G., Min I. – S., Kim W. – T., *Solid state communications*, 64 (5) (1987), 819.

[38] Kim N. – O., Kim H. – G., Lim H. – J., Lee C. –I., Jin M. – S., Yoon C. – S., Kim W. – T., *J. Korean physical society*, 38 (4) (2001), 405.

[39] Bidjin D., Popovic S., Celustaka B., *Phys. Status Solidi (a)*, 6 (1971), 295.

[40] Ebnalwaled A. A., Gamal G. A., Elshaikh H. A., Mahasen M. M., *Journal of Applied Physical Science International*, 5 (1) (2016), 1.

[41] Mott N. F., Davis E. A., "Electronic Process in Non-Crystalline Materials", Clarendon, Oxford, 1979.

[42] Paul D. K., Mitra S. S., *Phys. Rev. Lett.*, 31 (1973), 1000.

[43] Ebnalwaled A. A., Al-Orainy R. H., *Appl Phys A*, 112 (4) (2013), 955.

[44] Seto J. Y., *J. Appl. Phys.*, 46 (1975), 5247.

[45] Borah M., Mohanta D., *Appl Phys A*, 115 (3), (2014), 1057.

[46] Murugaraj R., Govindaraj G., George D., *Mater. Lett.*, **57** (2003), 1656.

[47] Jonscher A. K., *J. Mater. Sci.*, 16 (1981), 2037.

[48] Pike G. E., *Phys. Rev. B*, **6** (1972), 1572.

[49] Ebnalwaled A. A., *International journal of Basic & Applied Sciences*, 11 (6) (2011), 194.

[50] Ebnalwaled A. A., *Mater. Sci. Eng. B*, 174 (1-3) 25 (2010), 285.

[51] Al-Orainy R. H., Nagat A. T., Hussein S. A., Ebnalwaled A. A., *International Research Journal of Engineering and Technology*, 2 (2) (2015), 816.

[52] Austin I. G., Mott N. F., *Adv. Phys.*, 18 (1969), 41.

[53] Bekheet A. E., *Physica B*, 403 (2008), 4342.

[54] Hegab N. A., Afifi M. A., Atyia H. E., Farid A. S., *J. Alloys Compd.*, 477 (2009), 925.

[55] Xu L., Liu Y., Chen B., Zhao C., Lu K., *Polymer Composites*, 34 (10) (2013), 1728.

[56] Cui J., Wang L., Du Z., Ying P., Deng Y., *J. Mater. Chem. C.*, 3 (2015), 9069.

[57] Cui J. L., Zhang X. J., Deng Y., Fu H., Yan Y. M., Gao Y. L., Li Y. Y., *Scripta Materialia*, 64 (2011), 510.

[58] Wilson A. H., Theory of Metals, 2nd edition, Cambridge University press, Cambridge, 1953.

[59] Gamal G. A., Abou Zied M., Ebnalwaled A. A., *Physica B*, 393 (2007), 285.

[60] Pang E. J. X., Pickering S. J., Chan A., Wong K. H., Lau P. L., *Journal of Solid State Chemistry*, 193 (2012), 147–153.